Extent of Lateral Epidermal Protection Afforded by A Cryogen Spray Against Laser Irradiation

Walfre Franco, PhD,[1,2]* Jie Liu, MS,[1] Ricardo Romero-Méndez, PhD,[1,3] Wangcun Jia, PhD,[2] J. Stuart Nelson, MD, PhD,[2] and Guillermo Aguilar, PhD[1,2]

[1]*Department of Mechanical Engineering, University of California, Riverside, California 92521*

[2]*Beckman Laser Institute, University of California, Irvine, California 92612*

[3]*Facultad de Ingeniería, Universidad Autónoma de San Luis Potosí, México*

Background and Objectives: Cryogen spray cooling (CSC) has become an integral part of dermatologic laser surgery because of its ability to remove selectively large amounts of heat from human skin in short periods of time, thereby protecting the epidermis from unintended thermal injury. The objective of the present study is to investigate the extent of lateral epidermal protection afforded by a cryogen spray during laser irradiation.

Materials and Methods: CSC experiments on skin phantoms are conducted using a commercial nozzle (GentleLase, Candela) to characterize epidermal cooling in time and space; namely, surface temperatures and heat fluxes during a 60 milliseconds spurt and 30 milliseconds delay. Numerical methods are used to model the light distribution (755 nm), heat diffusion and thermal injury within the epidermis and dermis. A 755 nm laser (GentleLase, Candela) was used to assess in vivo the extent of lateral epidermal protection against irradiation in human skin.

Results: The commercial nozzle produced an uneven deposition and spread of liquid cryogen, thereby creating zones of high and low heat extraction on the surface. Numerical and in vivo studies show that 18 mm diameter laser beams may induce skin injury at the periphery of the irradiated areas. However, a 10 mm diameter beam provides the safest therapy because only the zone of highest heat extraction is exposed to laser irradiation. Beyond 10 mm, heat extraction is no more than a third of the maximum heat extraction within this diameter.

Conclusions: Accumulation of heat within the epidermis is always greater at the laser beam periphery, away from the CSC nozzle tip, where heat extraction is lowest. Therefore, there is risk of thermal injury at the beam periphery when there is a mismatch between the skin protected by CSC and that exposed to laser irradiation. For the cooling and irradiation sequences considered herein, heat extraction provided by a 60 milliseconds spurt/30 milliseconds delay correctly matches the heating profile of a 10 mm diameter beam. Lasers Surg. Med. 39:414–421, 2007. © 2007 Wiley-Liss, Inc.

Key words: laser therapy; epidermal protection; dynamic cooling; heat transfer; spatial dynamics

INTRODUCTION

Prior to laser irradiation, cryogen spray cooling (CSC) is applied to lower the temperature in the epidermis in order to prevent injury due to unintended, uncontrolled, excessive heating therein [1,2]. The physics of liquid evaporating sprays, such as CSC are inherently complex: for example, within a single cryogen spray there are wide ranges in droplet size and velocity that are functions of time, space, nozzle geometry and atmospheric conditions [3]. It follows that heat extraction from the epidermis during CSC is time and space dependent; hence, a better understanding of the heat flux profile during CSC of human skin would allow the selection of appropriate laser beam diameters, thereby matching the zones of epidermal cooling and heating.

There are many studies on the time and space-dependent heat transfer of CSC, nozzle geometries, surface-nozzle distances, and spurt durations [4,5], yet only a few have addressed lateral variations in heat transfer [4,6,7]. Franco et al. [8] showed that temporal and spatial variations in heat extraction from a skin phantom during CSC are significant and, consequently, epidermal protection provided by CSC is not uniform. These studies considered vertical sprays produced by nozzles at 90° with respect to the horizontal plane. However, in clinical practice nozzles are angled approximately 100–120° with respect to the skin surface. A recent study showed that a 15° angle difference (105° as opposed to 90°) led to negligible differences in heat transfer during CSC [9]; however, the heat flux measurements were only taken at the center of the sprayed surface, and differences in heat flux as large as 250 kW/m^2 with respect to the periphery have been reported [9]. This issue becomes particularly relevant in light of a report of patients with ring and crescent-shaped skin burns after CSC-assisted laser procedures [10], highlighting the significance

Contract grant sponsor: National Institutes of Health; Contract grant numbers: AR47551, AR48458, GM62177, HD42057.

*Correspondence to: Walfre Franco, PhD, Beckman Laser Institute, 1002 Health Science Road East, Irvine, CA 92612
E-mail: wfranco@uci.edu

Accepted 21 March 2007
Published online 18 June 2007 in Wiley InterScience (www.interscience.wiley.com).
DOI 10.1002/lsm.20511

of investigating the thermal response of the epidermis over the entire area exposed to laser irradiation.

MATERIALS AND METHODS

Experimental Methods

Spray system. The spray system [9] uses a valve from a commercial handpiece (GentleLase, Candela, Wayland, MA), which has an angled tube-nozzle at 120°, to deliver a single 60 milliseconds cryogen spurt 30 mm away from the phantom surface.

Thermal sensors. The thermal sensor consists of four type-K thermocouples (CHAL-005, Omega, Stamford, CT) soldered to a linear array of four silver discs (1 mm diameter, 0.09 mm thickness with 1 mm separation between discs) embedded in an epoxy resin, as described in [11]. The diameter of the thermocouple wires is 125 μm and the bead diameter is approximately 300 μm. According to the manufacturer, the thermal response of a similar type-J thermocouple in still water is 40 milliseconds. Since the thermocouple response is a function of the immersion medium, alloy type and temperature, a much faster response is expected with liquid cryogen. The sensor is displaced laterally to measure temperature variations along the largest diameter (or long axis of an irregular ellipse) of the sprayed surface. A flexible heater attached to the bottom of the phantom provides a continuous heat flux such that the steady state temperature at the top surface is ≈31°C.

Numerical Methods

Surface heat flux computation. Temperatures recorded by the thermal sensor are assumed to be surface temperatures because the silver disc Biot number (hL/k) for a heat transfer coefficient $h = 20{,}000$ W/m^{2}K [12], characteristic length $L = 0.09\times10^{-3}$ m and thermal conductivity $k = 429$ W/m K is ≈0.004; that is, the disc temperature is spatially uniform, $hL/k << 1$. The following analytical expression based on Fourier's law and Duhamel's theorem is used to compute the surface heat flux q_c from temperature measurements θ:

$$q_c(t_I) = 2\sqrt{\frac{k\rho c}{\pi}}\sum_{i=1}^{I}\frac{\theta_i - \theta_{i-1}}{\sqrt{t_I - t_i} + \sqrt{t_I - t_{i-1}}}, \qquad (1)$$

where t is the time and I the total number of measurements. A detailed derivation of Eq. (1) can be found in [8,13]. The total heat extraction H is the time integral of q_c.

Modeling light distribution. The Monte Carlo method of steady-state light transport in multi-layered tissue MCML [14] and its corresponding convolution program CONV [15] are used to model photon distribution and calculate the radiant energy deposition $Q_{L,i}$. It is assumed that the epidermis has a melanosome absorption coefficient of 17,000 m^{-1} at 755 nm [16], a baseline absorption coefficient of 25 m^{-1} and a melanin volume fraction of 10%, which corresponds to a moderately pigmented skin phototype. It is also assumed that the dermis has a 1% blood volume fraction and that the blood absorption coefficient is 303 m^{-1} [17]. Absorption (μ_a) and scattering (μ_s) coefficients of the epidermis and dermis are computed following [18], and the anisotropy factor (g) is computed following [19]. Thermal [8] and optical properties of human skin [16–19] are shown in Table 1; scattering coefficients and anisotropy factors of the epidermis and dermis are assumed to be the same. Energy deposition is computed for three different flat top laser beams of 10, 14, and 18 mm diameters and 16, 31, and 51 W powers, respectively, such that the radiant exposure of each beam is maintained constant at approximately 20 J/cm^2 for a 3 milliseconds pulse.

Modeling temperature response. The heat transfer equation for in vivo human skin can be expressed as

$$\rho_i c_i \frac{\partial}{\partial t}T_i(x,z,t) - \nabla(k_i\nabla T_i(x,z,t)) = \rho_b c_b \omega_i (T_b - T_i(x,z,t)) + Q_{m,i} + Q_{L,i}, \qquad (2)$$

where subindices i and b denote, respectively, tissue type (e for epidermis and d for dermis) and blood, ρ is density ($\rho_b = 1{,}100$ kg/m^3 and $c_b = 3{,}600$ J/kg/K), c is specific heat, T is temperature, k is thermal conductivity, ω is average volumetric blood perfusion rate per unit tissue volume (3×10^{-3} per second for the epidermis and 6×10^{-3} per second for the dermis), T_b (37°C) is the blood (core-body) temperature of untreated blood vessels, and Q_m (400 W/m^3) and Q_L are, respectively, heat sources from metabolism and radiant energy deposition. The first term on the right side of Eq. (2) accounts for the effect of blood perfusion and the last term accounts for photon absorption by chromophores in the tissue, which is zero before and after laser exposure. The initial temperature of the epidermis and dermis is 37°C. The computational domain is $0\le x\le 50\times10^{-3}$ and $0\le z\le 1.505\times10^{-3}$ m; the epidermis is within $0\le z\le 0.05\times10^{-3}$ m. At the skin surface, the thermal boundary condition is

$$-\mathbf{n}\cdot k\nabla T_e(x,0,t) = \begin{cases} q_c(x,t) & \text{if } t \le t_c, \\ h(\theta - T_\infty) & \text{if } t > t_c, \end{cases} \qquad (3)$$

where $\mathbf{n}$ is the unit vector normal to the surface, t_c is the cooling time, and h is the heat transfer coefficient. Assuming that similar temperature dynamics can be imposed on human skin during CSC as those observed in the skin phantom, q_c is computed from Eq. (1). During

TABLE 1. Thermal [8] and Optical Properties of Human Skin[16–19]

	c (J/kg K)	ρ (kg/m^3)	k (W/m K)	μ_a (1/m)	μ_s (1/m)	g	n
Epidermis	3,600	1,200	0.21	1,800	15,800	0.79	1.37
Dermis	3,800	1,200	0.53	310	15,800	0.79	1.37

laser irradiation and thereafter, $t > t_c$, air flows over the skin surface, for which the free convection boundary condition is modeled using $h = 150$ W/m/K of air flowing over a hot plate [20]. At the other boundaries, the zero-flux boundary condition is

$$\mathbf{n} \cdot \nabla T_i(x, z, t) = 0. \quad (4)$$

The finite element method (Comsol, Burlington, MA) is used to solve Eqs. (2–4).

Modeling thermal injury. The Arrhenius rate process model of thermal injury is used to evaluate the depth and lateral extent of epidermal injury, and as a criterion for comparison between exposures using different laser beam diameters. Thermal injury within the epidermis $\Omega(x, z)$ can be expressed as

$$\Omega = A \int_0^t \exp\left(-\frac{E_a}{RT_e(x, z, \tau)}\right) d\tau, \quad (5)$$

where A (1.8×10^{51} 1/second) is the frequency factor, E_a (327×10^3 J/mole) is the activation energy threshold and R (8.32 J/mole/K) is the universal time constant [21]. Since the dermis has a low absorption coefficient at 755 nm, deposition of radiant energy therein is very small in comparison to that in the epidermis; thus, if the epidermis is not injured, neither is the dermis. Irreversible damage to the epidermis is assumed to occur when 63% or more of the tissue is injured; that is, $\Omega = 1$ [22]. Even though the computational domain is larger, computations of T and Ω are only shown for the epidermis wet by the spray: $0 \le x' \le 22 \times 10^{-3}$ m and $0 \le z \le 0.05 \times 10^{-3}$ m, where a linear transformation, $x' = x - 18$, is introduced to facilitate presentation and discussion; however, for brevity the prime is dropped. q_c before and after the wet surface is assumed to decrease down to zero toward the edges of the lateral domain, such that Eq. (4) is satisfied.

RESULTS

Temporal and Spatial Variations in Liquid Cryogen Deposition and Surface Heat Transfer During CSC. A series of images of a 60 milliseconds cryogen spurt on the skin phantom is shown in Figure 1. Image acquisition is simultaneous with temperature measurements, such that the spatial distribution of the liquid can be correlated with surface heat extraction from the phantom. Measured valve opening and closing delays were 9 and 18 milliseconds, respectively—frames not shown. Figure 1a shows the initial in-flight droplets reaching the substrate; Figure 1b shows a fully developed spray cone of 6 mm diameter at the phantom surface; Figure 1c–h shows the uneven radial displacement of liquid cryogen on the phantom surface by the incoming spray. The longest length (or major axis of an irregular ellipse) sprayed surface is 22 mm along the direction of the sensor array (see Fig. 1a). The angled nozzle produces asymmetric deposition and spreading of liquid cryogen with respect to the x axis. As a result, the shape of the sprayed liquid cryogen is an irregular ellipse. In modeling, we consider temperature

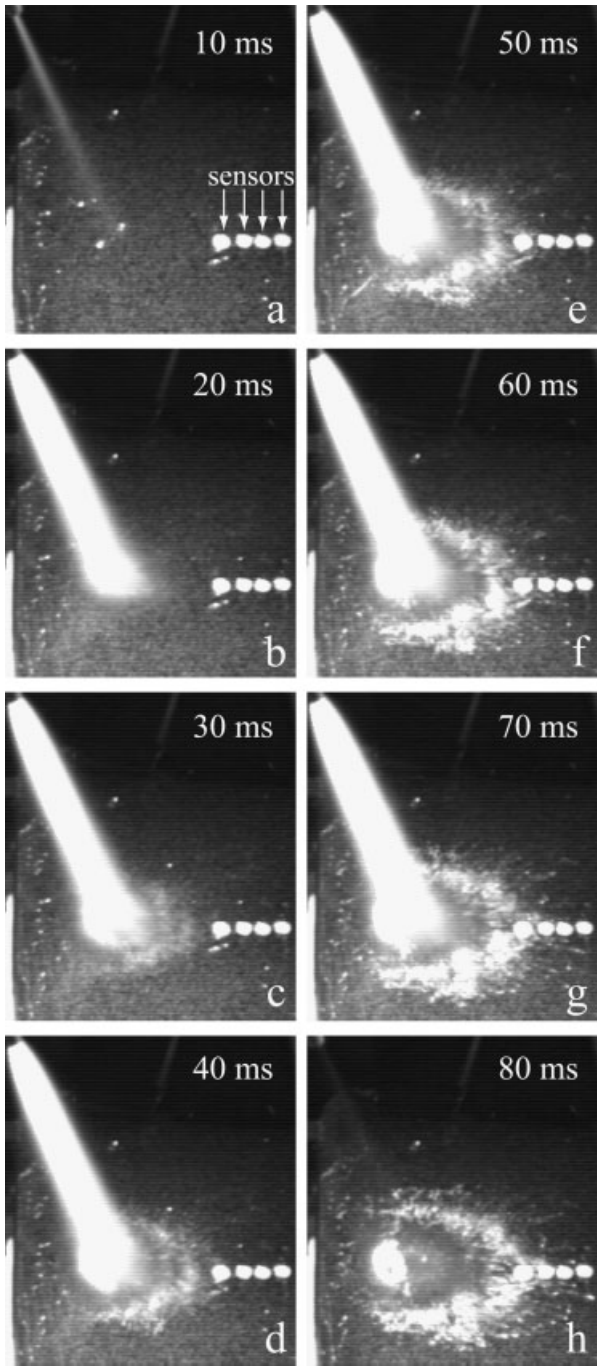

Fig. 1. CSC of a multiple-sensor skin phantom: 60 milliseconds spurt, 30 mm phantom-nozzle distance. Cryogen deposition (a) 10, (b) 20, (c) 30, (d) 40, (e) 50, (f) 60, (g) 70 and (h) 80 ms after valve is enersized.

variations along x; that is, the major axis of the irregular ellipse.

θ, q_c, and H' (normalized total heat extraction) along the long axis (x) of the sprayed surface are shown in Figure 2. θ distributions are shown from 10 to 90 milliseconds in increments of 10 milliseconds in Figure 2a. q_c distributions

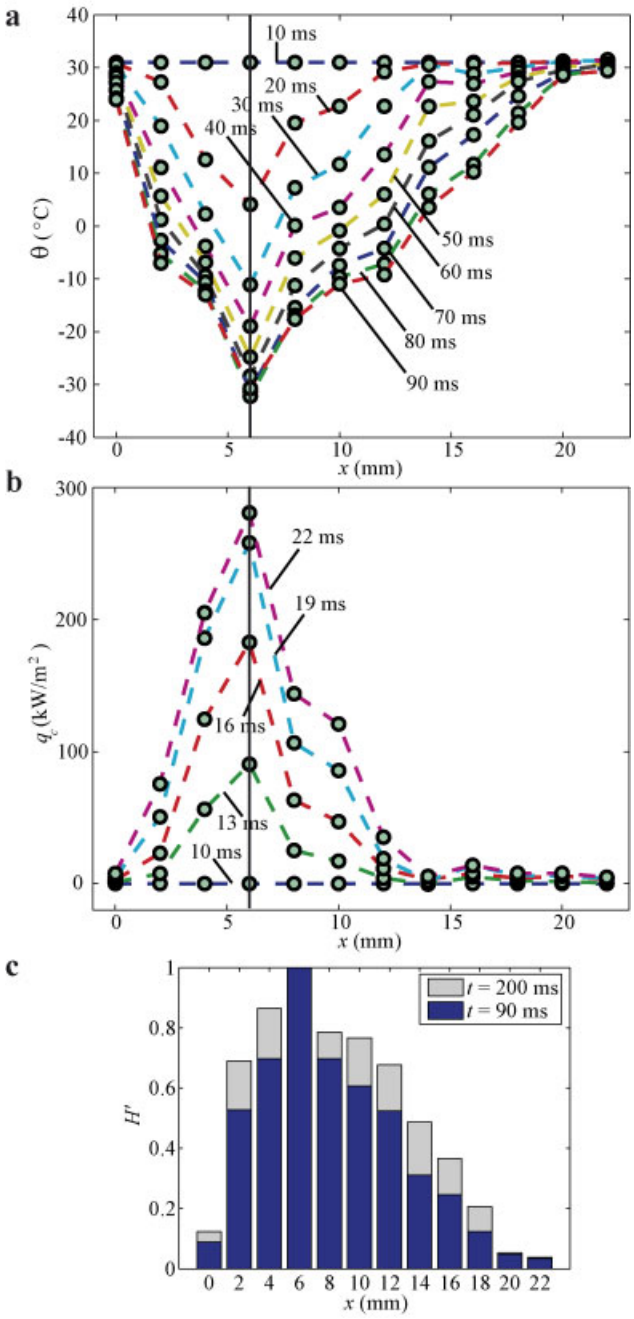

Fig. 2. Distributions of surface (**a**) temperature and (**b**) heat flux along the long axis of the sprayed surface at specific times during CSC: 60 milliseconds spurt, 30 mm phantom-nozzle distance. Vertical solid lines indicate location, $x = 6$ mm, of minimum θ and maximum qc. (**c**) Normalized total heat extraction at two different times: $H' = H/H_{x=6}$ and $H_{x=6} = 17.7$ J/m^2 and 25.5 J/m^2 at $t = 90$ and 200 milliseconds, respectively. [Figure can be viewed in color online via www.interscience.wiley.com.]

are shown in increments of 3 milliseconds from 10 to 22 milliseconds, the latter being the time when the maximum heat flux occurs in Figure 2b. H' distributions at 90 and 200 milliseconds are shown in Figure 2c. Distributions are normalized with respect to the maximum H at the time, which occurs at $x = 6$ mm. Further details of the temporal and radial evolutions of heat transfer during CSC can be found in Reference [8].

Thermal Variations Across the Epidermis During Laser Irradiation

When modeling laser therapy, it is intended that the laser beam irradiates the skin where the heat extraction is highest. Therefore, the centers of the 10, 14, and 18 mm diameter beams are, respectively, at $x = 7$, 9, and 11 mm because cooling is high at $x > 2$ mm in Figure 3a,b (i.e., laser beam centers at 2+5, 2+7, and 2+9 mm). The time sequence of modeling is a 60 milliseconds cryogen spurt, 30 milliseconds delay, 3 milliseconds laser pulse, and 80 milliseconds post-laser relaxation time.

Maps of temperature T within the epidermis after CSC-laser irradiation are shown in Figure 3. These cross-sectional maps correspond to the time ($t = 96$ milliseconds) when maximum T occurs. In Figure 3a ($T_{max} = 46$°C), there is a certain symmetry of heating with respect to the beam

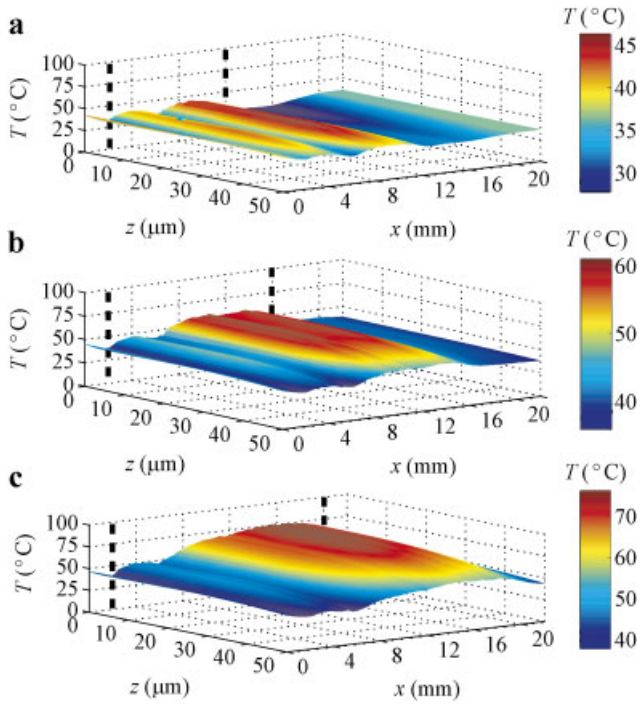

Fig. 3. Temperatures within epidermis after CSC-laser irradiation using laser beams of (**a**) 10, (**b**) 14 and (**c**) 18 mm diameters: 60 milliseconds cryogen spurt, 30 milliseconds delay, 3 milliseconds laser pulse, 20 J/cm^2 radiant exposure, 755 nm wavelength. Vertical dashed lines illustrate irradiation diameter. [Figure can be viewed in color online via www.interscience.wiley.com.]

central axis, $x = 7$ mm. In Figure 3b ($T_{max} = 61°C$), heating is asymmetric and regions of higher temperatures exist towards the beam periphery at $x = 16$ mm. In Figure 3c ($T_{max} = 76°C$), heating is also asymmetric and even larger regions of higher temperatures exists towards the periphery at $x = 20$ mm.

Figure 4 shows contour maps of thermal injury Ω within the epidermis at $t = 170$ milliseconds, when accumulation of thermal injury has ceased to occur. Figure 4a,b shows that the 10 and 14 mm diameter beams irradiate from $x = 2–12$ and $x = 2–16$ mm without damaging the epidermis ($\Omega << 1$). Figure 4c shows that the 18 mm diameter beam, which irradiates within $x = 2–20$ mm, induces excessive injury at the periphery from $x \approx 13–19$ mm and that $\Omega >> 1$ from the surface to $z \approx 30$ μm.

DISCUSSION

Cryogen Liquid Deposition and Surface Heat Extraction

An angled nozzle produces uneven radial surface deposition and spreading of liquid cryogen, Figure 1a–h, which in turn induce a skewed thermal field with significant differences along the long axis of the sprayed surface, Figure 2. The liquid distribution corresponding to $t = 90$ milliseconds is shown in Figure 5a, where three zones (A–C) can be identified based on temperatures and the appearance of the liquid cryogen on the surface: a clearly defined inner region (≈10 mm) called the high heat extraction zone A for which drops in θ are $> 40°C$ ($r = 2–12$ mm in Fig. 2a); the region covered homogeneously by the liquid film (≈18 mm) called the wet zone B, which corresponds to small drops in θ beyond A (≈10°C at $r = 0$ and 18 mm in Fig. 2a); and, the region covered inconsistently by liquid cryogen columns (≈22 mm) called the crown-shaped zone C, where drops in θ beyond B are insignificant (≈4°C at $r = 20$ and 22 mm in Fig. 2a). These zones are better appreciated in Figure 5b, which displays dispersion of liquid cryogen at $t = 90$ milliseconds on a Plexiglas® surface imaged from below.

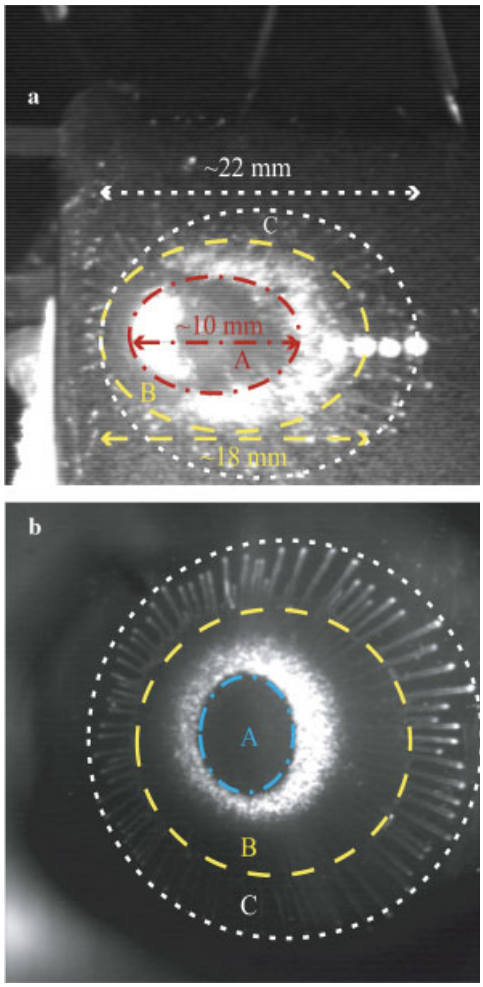

Fig. 5. Liquid cryogen spread at $t = 90$ milliseconds on (**a**) the skin phantom and (**b**) a Plexiglas® substrate; the high heat extraction, wet and crown-shaped zones are labeled: A, ---; B, --; –C, ···; respectively. [Figure can be viewed in color online via www.interscience.wiley.com.]

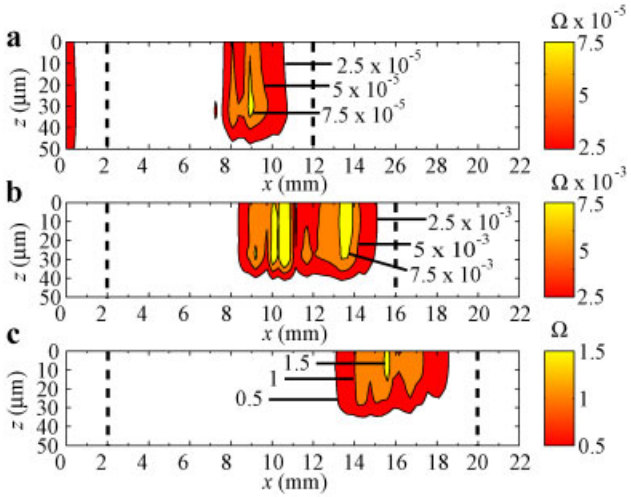

Fig. 4. Contour maps of thermal damage Ω within the epidermis after CSC-laser irradiation using laser beams of (**a**) 10, (**b**) 14, and (**c**) 18 mm diameters: 60 milliseconds cryogen spurt, 30 milliseconds delay, 3 milliseconds laser pulse, 20 J/cm^2 radiant exposure, 755 nm wavelength. Vertical dashed lines illustrate irradiation diameter. [Figure can be viewed in color online via www.interscience.wiley.com.]

Extent of Lateral Epidermal Protection by CSC Against Laser Heating

The 10 mm diameter laser beam irradiates zone A within the sprayed surface without excessive epidermal heating, Figures 3a and 4a. The 14 and 18 mm diameter beams

irradiate the sprayed surface outside zone A, which leads to significantly higher temperatures and two and three orders of magnitude increase in Ω, respectively, Figures 3b,c and 4b,c. Weisberg and Greenbaum [10] reported rings and crescent-shaped marks of hyperpigmented skin after CSC-assisted laser hair removal on patients with different skin phototypes. Although the laser radiant exposure was individually adjusted, these authors used a 50 milliseconds spurt/50 milliseconds delay and an 18 mm laser beam diameter on all patients. Dyspigmentation by cooling is unlikely because the drop in temperature at the sprayed zone periphery is insignificant, Figure 2a. Kelly et al. [23,24] demonstrated experimentally that there is risk of thermal injury if the spurt duration is too short, the handpiece is not held perpendicular to the skin surface, or the cryogen nozzle is misaligned. Furthermore, even if these situations could be avoided, the results of the latter investigation showed that there is also a risk of skin injury by excessive heating if there is a mismatch between the skin surface protected by CSC and that exposed to laser irradiation. Figure 5a suggests that if the laser beam diameter matches the area covered by the wet zone B (beyond the highest heat extraction zone A) then there is risk of skin injury manifested as crescent-shaped burns due to excessive heating. There is little or no risk of skin injury by cooling within the wet zone and beyond since the heat extraction therein is low ($H' \leq 0.31$ for $x > 12$ mm, Fig. 2c) and the minimum temperatures reached are high ($\theta > 0^{\circ}C$ for $x > 12$ mm at $t = 90$ milliseconds, Fig. 2a). It is important to note that the heat transfer and fluid mechanics of CSC are highly dynamic; hence, *the extent of the protected skin surface is also time and space-dependent*. Figure 2c shows that $H' \approx 0.3$ at $x = 14$ mm and $t = 90$ milliseconds, and that $H' \approx 0.5$ at the same location and $t = 200$ milliseconds.

Figure 6 shows dermatoscope images of a volunteer with skin phototype III 24 hours after exposure to 10 and 18 mm diameter laser beams; 50 milliseconds cryogen spurt/50 milliseconds delay, 20 J/cm^2 laser radiant exposure (GentleLase, Candela; wavelength 755 nm; pulse duration 3 milliseconds). Figure 6a shows few, scattered crusts on the skin surface within the 10 mm diameter irradiated area. These crusts, which eventually exfoliate, result from blood within the dermis leaking to the skin surface due to an injured epidermis. Figure 6b shows several crusts on the skin surface that are larger in size and clustered at the periphery of the 18 mm diameter irradiated area. Figure 7 shows images 24 hours after exposure to 50/30 and 60/30 milliseconds cooling sequences; 18 mm laser beam diameter, 20 J/cm^2 laser radiant exposure. Figure 7a shows a similar distribution of crusts on the skin surface as in Figure 6b but the crusts are not as numerous. Figure 7b shows a significant reduction in crusts on the skin respect to Figures 6b and 7a. The location of the nozzle valve in Figures 6 and 7 corresponds to the left of the image; that is, the largest axis of the sprayed surface runs from left to right, as in Figure 1.

A 10 mm diameter laser beam is a better suited for a 50/50 milliseconds cooling sequence than an 18 mm diameter beam, Figure 6a,b. For the subject's skin phototype and the CSC and laser parameters considered herein, there is a ring/crescent-shaped mismatch between cooling and heating irradiating over an 18 mm diameter area, Figures 6b and 7a. As proposed previously [24], increasing the spurt duration can enhance the extent of lateral epidermal protection afforded by CSC: Figure 7b shows that a 60/30 milliseconds cooling sequence provides for more skin protection than 50/50 and 50/30 milliseconds sequences. Adjusting the time delay between CSC and irradiation can also enhance protection [8]: Figures 6b and 7a show that a 50 milliseconds delay resulted in more crusting as opposed to using a shorter 30 milliseconds delay. It is reasonable to

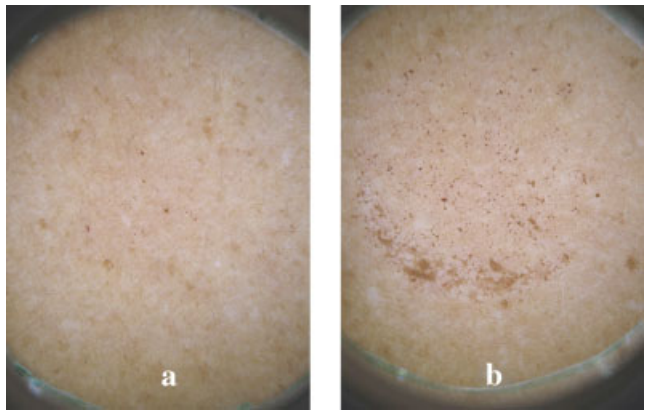

Fig. 6. Skin phototype III 24 hours after 755 nm, 3 milliseconds, 20 J/cm^2 laser exposure to (**a**) 10 and (**b**) 18 mm diameter laser beams. CSC: 50 milliseconds spurt/50 milliseconds delay before laser exposure. [Figure can be viewed in color online via www.interscience.wiley.com.]

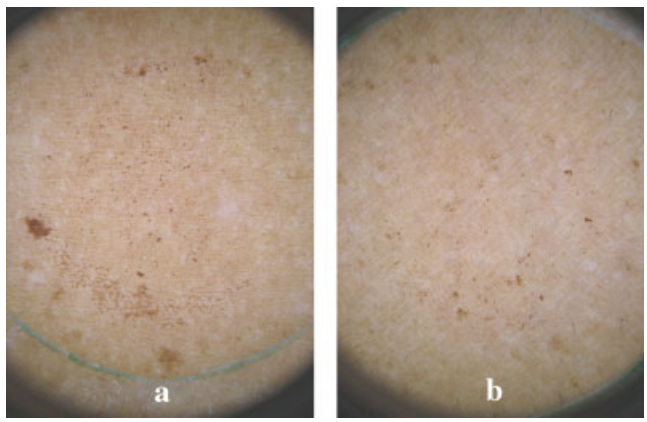

Fig. 7. Skin phototype III 24 hours after 755 nm, 3 milliseconds, 20 J/cm^2 laser exposure to 18 mm diameter laser beams. CSC: (**a**) 50 milliseconds spurt/30 milliseconds delay before laser exposure; (**b**) 60 milliseconds spurt/30 milliseconds delay before laser exposure. [Figure can be viewed in color online via www.interscience.wiley.com.]

expect lower CSC protection at the periphery of the irradiated area in Figure 6b; however, there is crusting on the skin surface at the center of the beam. Light from the periphery of the incident beam partly scatters inwards towards the beam axis increasing the deposition rate at the middle of the beam [25]; that is, even though the radiant exposure of the 10 and 18 mm beams is the same, there are more photons deposited in the middle of the 18 mm beam.

To extend the epidermal protection provided by CSC, the use of an array of nozzles may be explored. Alternatively, modifying the fluid structure of the spray itself may produce a more uniform thermal field and higher epidermal protection; for example, swirling sprays to induce different impinging patterns, or sprays released in controlled environments at reduced humidity and pressure [26–28] to reduce ice formation and obtain a finer spray (smaller cryogen droplet size). Finally, a quite simple implementation for future handpiece designs is to aim the spray tube-nozzle directly perpendicular to the skin surface.

CONCLUSIONS

Experiments with CSC on skin phantoms were used to correlate cryogen liquid distribution with surface heat transfer, and obtain space and time-dependent boundary conditions to model the thermal response of the epidermis to CSC-assisted laser procedures using laser beams of different diameters. In vivo experiments were carried out to compare the skin response to laser beams of different diameters. Angled spray nozzles induce asymmetric heat extraction along the major axis of an (irregular) elliptical sprayed surface and, consequently, asymmetric epidermal protection; there is a high heat extraction zone within the sprayed surface where epidermal protection is maximal, this zone is not evident and its size is time and space-dependent. There is risk of injury when there is a mismatch between the skin protected by CSC and that exposed to laser irradiation. Because of the time and space-evolution of cooling imposed by the spray, accumulation of heat within the epidermis is always greater at the laser beam periphery where heat extraction by CSC is lowest. The use of a 10 mm diameter laser beam with CSC reduces the risk of epidermal injury, and longer spray durations should be used with 18 mm diameter laser beams to reduce the risk of epidermal injury at the periphery of the beam.

ACKNOWLEDGMENTS

This work was supported by the following grants from the National Institutes of Health: AR47551, AR48458 and GM62177 to JSN and HD42057 to GA. Presentation of part of this work at the 2005 Annual Meeting of the American Society for Laser Medicine and Surgery was supported by a travel grant from the United States Air Force Office of Scientific Research to WF. Research support provided by Dr. Julio Ramírez San Juan is greatly appreciated.

REFERENCES

1. Nelson JS, Milner TE, Anvari B, Tanenbaum BS, Kimel S, Svaasand LO, Jacques SL. Dynamic epidermal cooling during pulsed-laser, treatment of port-wine stain—A new methodology with preliminary clinical-evaluation. Arch Dermatol 1995;131(6):695–700.
2. Nelson JS, Milner TE, Anvari B, Tanenbaum BS, Svaasand LO, Kimel S. Dynamic epidermal cooling in conjunction with laser-induced photothermolysis of port wine stain blood vessels. Lasers Surg Med 1996;19(2):224–229.
3. Lefebvre AH. Atomization and sprays. 1989. New York: Taylor & Francis.
4. Aguilar G, Majaron B, Pope K, Svaasand LO, Lavernia EJ, Nelson JS. Influence of nozzle-to-skin distance in cryogen spray cooling for dermatologic laser surgery. Lasers Surg Med 2001;28(2):113–120.
5. Aguilar G, Majaron B, Karapetian E, Lavernia EJ, Nelson JS. Experimental study of cryogen spray properties for application in dermatologic laser surgery. IEEE T Bio-Med Eng 2003;50(7):863–869.
6. Verkruysse W, Majaron B, Aguilar G, Svaasand LO, Nelson JS. Dynamics of cryogen deposition relative to heat extraction rate during cryogen spray cooling. In SPIE's International Symposium, Photonics West. 1999; San Jose, CA.
7. Choi B, Welch AJ. Infrared imaging of 2-D temperature distribution during cryogen spray cooling. J Biomech Eng-T ASME 2002;124(6):669–675.
8. Franco W, Liu J, Wang GX, Nelson JS, Aguilar G. Radial and temporal variations in surface heat transfer during cryogen spray cooling. Phys Med Biol 2005;50(2): 387–397.
9. Aguilar G, Vu H, Nelson JS. Influence of angle between the nozzle and skin surface on the heat flux and overall heat extraction during cryogen spray cooling. Phys Med Biol 2004;49(10):N147–N153.
10. Weisberg NK, Greenbaum SS. Pigmentary changes after alexandrite laser hair removal. Dermatol Surg 2003;29(4): 415–419.
11. Franco W, Wang GX, Nelson JS, Aguilar G. Effect of surface thermal variations during cryogen spray cooling in dermatologic laser therapy. In 17th Annual Conference ILASS-Americas. 2004; Washington, DC.
12. Jia WC, Aguilar G, Wang GX, Nelson JS. Heat-transfer dynamics during cryogen spray cooling of substrate at different initial temperatures. Phys Med Biol 2004;49(23): 5295–5308.
13. Beck JV, Blackwell B, St. Clair CR, Jr. Inverse heat conduction: Ill posed problems. 1985. New York: Wiley.
14. Wang LH, Jacques SL, Zheng LQ. MCML—Monte-carlo modeling of light transport in multilayered tissues. Comput Meth Prog Bio 1995;47(2):131–146.
15. Wang LH, Jacques SL, Zheng LQ. CONV—Convolution for responses to a finite diameter photon beam incident on multi-layered tissues. Comput Meth Prog Bio 1997;54(3):141–150.
16. Jacques SL, McAuliffe DJ. The melanosome—Threshold temperature for explosive vaporization and internal absorption-coefficient during pulsed laser irradiation. Photochem Photobiol 1991;53(6):769–775.
17. Prahl, S, Optical Absorption of Hemoglobin. 1999 http://omlc.ogi.edu/spectra/hemoglobin/summary.html.
18. Jacques, SL, Skin optics. 1998 http://omlc.ogi.edu/news/jan98/skinoptics.html.
19. Svaasand LO, Norvang LT, Fiskerstrand EJ, Stopps EKS, Berns MW, Nelson JS. Tissue parameters determining the visual appearance of normal skin and port-wine stains. Laser Med Sci 1995;10(1):55–65.
20. Holman JP. Heat transfer. 1981. New York: McGraw Hill.
21. Weaver JA, Stoll AM. Mathematical model of skin exposed to thermal radiation. Aerosp Med 1969;40(1):24–30.
22. Pearce J, Thomsen S. Rate process analysis of thermal damage, in optical-thermal response of laser-irradiated tissue. AJ, Welch, MJC van Gemert. editors. 1995. New York: Plenum Publishing.

23. Kelly KM, Svaasand LO, Nelson JS. Optimization of laser treatment safety in conjunction with cryogen spray cooling. Arch Dermatol 2003;139(10):1372–1373.
24. Kelly KM, Svaasand LO, Nelson JS. Further investigation of pigmentary changes after alexandrite laser hair removal in conjunction with cryogen spray cooling. Dermatol Surg 2004; 30(4):581–582.
25. Keijzer M. Light transport for medical laser treatments, in Department of Technical Mathematics and Informatics. 1993. Delft University of Technology: Delft.
26. Majaron B, Kimel S, Verkruysse W, Aguilar G, Pope R, Svaasand LO, Lavernia EJ, Nelson JS. Cryogen spray cooling in laser dermatology: Effects of ambient humidity and frost formation. Lasers Surg Med 2001;28(5):469–476.
27. Franco W, Liu J, Aguilar G. Fluid mechanics and heat transfer of cryogen sprays applied to human skin under vacuum pressures. In Third International Conference on Fluid Structure Interaction. 2005; Coruña, Spain.
28. Ramirez-San-Juan JC, Choi B, Franco W, Nelson JS, Aguilar G. Effect of ambient humidity on light transmittance through skin phantoms during cryogen spray cooling. Phys Med Biol 2006;51(1):113–120.